SAND2017-9414C

Modeled Electroformed MEMS Variable Capacitor for Cobalt Iron Alloy Magnetostriction Measurements

E. D. Langlois[1], P. S. Finnegan[2], J. R. Pillars[3], T. C. Monson[4], M. H. Balance[5], C. R. St John[3], C. J. Pearce[4], A. J. Thorpe[3]

1. MEMS Technologies, Sandia National Laboratories, Albuquerque, NM, USA
2. Organic Materials Science, Sandia National Laboratories, Albuquerque, NM, USA
3. Physics Based Microsystems, Sandia National Laboratories, Albuquerque, NM, USA
4. Nanoscale Sciences Department, Sandia National Laboratories, Albuquerque, NM, USA
5. III-V Optoelectronics, Sandia National Laboratories, Albuquerque, NM, USA

Abstract: Electroplated CoFe alloys demonstrating Joule magnetostriction (i.e., a change in material shape induced by an applied magnetic field) have been recently developed at Sandia National Laboratories. A novel MEMS variable capacitor for measuring the magnetostriction as a function of applied magnetic field has been built in COMSOL® version 5.3. This model incorporates MEMS-scale electroformed mechanical and electrical features as well as the electrodeposited magnetostrictive alloy film under test. Simulations include displacement measurements of the capacitor under an applied magnetic field and the resulting change in capacitance. The MEMS variable capacitor has a modeled sensitivity of 0.48 (μm/pF) that can cover a range of 1 to 100 ppm of magnetostriction for a given geometry and material thickness.

1. Introduction

The incorporation of magnetostrictive materials in MEMS devices has been limited to either RF sputter deposited films such as Terfenol-D [$(Dy_{0.7}Te_{0.3})Fe_2$] [1, 2], CoFe [3], Galfenol (FeGa, FeGaB) [4, 5], and Mu-metal (NiFeCu) [6] or photochemical machining (PCM) of thick foils of as-cast Metglas™ 2826MB (amorphous $Fe_{40}Ni_{38}Mo_4B_{18}$ alloy) [7]. Both of these techniques have their drawbacks. RF sputter deposited materials, in general, suffer from a high degree of intrinsic stress, slow deposition rates, and lack compatible anisotropic etch processes to achieve vertically patterned sidewalls in thicker films. Photochemical machined foils are difficult to bond to standard micromachined films making their use for batch fabrication problematic. They also share the same problem as RF sputtered films where a high degree of isotropic lateral etching limits minimum feature sizes.

At Sandia National Laboratories, we have developed a novel electrodeposition technique capable of producing CoFe alloys that possess a high degree of saturation magnetostriction (λ_S = 78 ppm measured by the Naval Research Labs) as compared to commercial Metglas™ 2826MB (λ_S = 12 ppm). This technique provides a thick, in situ patterned, low intrinsic stress (10MPa) film that is deposited at low temperature (50°C). This technique can also produce batch fabricated arrays of patterned microstructures across multiple substrate materials. Finally, films with controllable phase and microstructure are possible without a high temperature (700-800°C) annealing step.

λ_S and $d_{33,\,m}$, the saturation magnetostriction and piezomagnetic coefficient, respectively, are fundamental performance metrics for magnetostrictive materials. Designing MEMS devices using magnetostrictive materials requires accurate measurements of these values in order to match modeled performance. Our solution for measuring magnetostrictive strain for electrodeposited films is to create a MEMS tunable capacitor that can be placed in any available magnetic source of high enough field strength to saturate the film. This paper covers the theory, design and modeling behind this unique device.

2. Theory and Design Features

One current method used for measuring thin film magnetostriction is by depositing the film on a non-magnetic cantilever and measuring its tip displacement under an applied magnetic field. Parallel ($D_{\parallel}$) and perpendicular ($D_{\perp}$) cantilever tip displacements from measurements with two orthogonal field directions are used to calculate an effective magnetostriction constant (λ_{eff}) using the expression of du Tremolet de Lacheisserie and Peuzin [8]:

$$\lambda_{eff} = \frac{2(D_{\parallel} - D_{\perp})E_s t_s^2 (1+\nu_f)}{9E_f L^2 t_f (1+\nu_s)} \qquad (1)$$

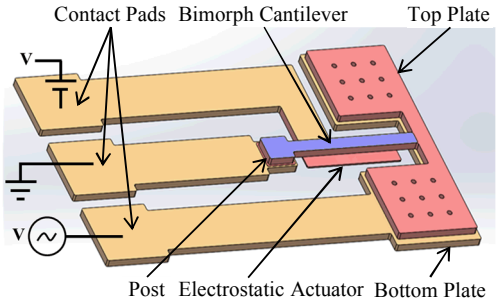

Figure 1. 3D rendering of a MEMS variable capacitor.

where L is the sample length, E_f and E_s are Young's moduli of the film and substrate, t_f and t_s are their respective thicknesses, and ν_f and ν_s are their respective Poisson′s ratios. For our device, the top plate of a tunable capacitor is attached to a cantilever tip and is paired with a stationary bottom plate where an electrical capacitance is measured and related back to the displacement via a modeled displacement vs. capacitance curve. Our cantilevers are 400 μm long, 40 μm wide, and 11 μm thick. A 3D conceptual rendering of our design is shown in Figure 1. We will refer to this device from here on out as MEMS Cap 1.

Table 1: Important device features, geometry and material composition.

Device Feature	Geometry	Material
Electrostatic Actuator	Width: 300 μm Depth: 80 μm Height: 4μm	Cu
Bimorph Cantilever: Top Film	Width: 400 μm Depth: 40 μm Height: 2μm	$Co_{70}Fe_{30}$
Bimorph Cantilever: Bottom Film	Width: 400 μm Depth: 40 μm Height: 9μm	Cu
Top Capacitor Plate	Area: 0.135 mm^2 Height: 9μm	Cu
Bottom Capacitor Plate	Area: ~0.16 mm^2 Height: 9μm	Cu
Air Volume	Sphere: R = 1.2 mm	Air

A top plate formed from the same copper layer as the cantilever provides the capacitance element of the device allowing a much smaller and stiffer mechanical structure. The size of the top plate was determined by both the magnitude and dynamic range of capacitance our device traverses as the cantilever bends under an applied magnetic field. An LCR meter is capable of detecting pF levels of capacitance with sufficient accuracy and two significant figures of resolution, hence, top plate areas corresponding to ~1pF levels of parallel plate capacitance were chosen. Larger top plate areas can be patterned to increase device capacitance but the decision must be weighed against the potential for stiction failure and will, therefore, ultimately be dictated by the success or failure of the sacrificial etch release.

The following section describes the COMSOL model for simulating magnetoelastic actuation for establishing an initial device design. The section also outlines steps used to set up the models including the physics, initial conditions, and boundary conditions.

3. Simulation

3.1. Geometry and Materials

Table 1 breaks down the various features of this device with regards to their geometry and material properties. All structures are designed to be made using electroformed metals with the exception of the electrostatic actuator electrode that may be simpler to create using thin film evaporation or sputter deposition techniques. The ultimate choice of metals used may also change depending on the ease of fabrication and other factors impacting the device functionality with the exception of the CoFe alloy layer. Specific material properties used for the modeling are listed in Appendix 1. Simple block shapes are used to create the various device features. The only exception is the hemispherical air volume which makes implementing Infinite Element domains simpler. The air volume scales dimensionally with the capacitor size and shape allowing for parametric sweeps without having to resize it every time there is a change in device geometry.

3.2. Physics Interfaces

Two different models were built to simulate the variable capacitor. The first model tackles the cantilever displacement and capacitance under electrostatic actuation. However, it will not be covered in this paper. The second model deals with cantilever displacement and capacitance under magnetoelastic bimorph actuation. The three physics interfaces used in this model are Solid Mechanics (*solid*) and Magnetic Fields (*mf*) with a Magnetostriction coupled interface (*pzm1*). The governing equations, initial conditions and boundary conditions used for solid mechanics interface are stated below.

Solid Mechanics (*solid*):

$$0 = \nabla \cdot S + F_V \tag{6}$$

where S is the stress tensor and F_V stands for the body force per volume. Initial conditions for the *solid* physics include the displacement field $u = (0, 0, 0)$ m

and the structural velocity field, $\delta u/\delta t$ = (0, 0, 0) m/s. Fixed constraints are applied at both the copper and CoFe alloy anchor point boundaries. The magnetic fields interface involves the following governing equations:

Magnetic Fields (*mf*):

$$\nabla \times H = J \quad (7)$$
$$B = \nabla \times (A_b + A_r) \quad (8)$$
$$J = \sigma E \quad (9)$$

where H is the magnetic field, J is the current density, B is the magnetic flux density, A_b is the background magnetic vector potential, A_r is the reduced magnetic vector potential, and σ is the electrical conductivity. Automatic values of A = (0, 0, 0) were applied for initial background flux conditions and a magnetic insulation condition, $n \times A = 0$, was applied to the outer boundary of the spherical air volume. A background magnetic vector potential, $A_b = B \cdot y$, is used to apply a constant magnetic flux along the x-axis as that also aligns to the easy axis of the modeled CoFe alloy film.

Magnetostriction (*pzm1*):

This multiphysics coupled interface is used to couple both the Solid Mechanics (*solid*) and Magnetic Fields (*mf)* interfaces exclusively on the CoFe alloy layer. The coupling type used is fully coupled. Use of the magnetostriction interface requires an additional node to both the Solid Mechanics (*solid*) and Magnetic Fields (*mf)* interfaces.

Magnetostrictive Material 1 is added to the Solid Mechanics (*solid*) interface to handle the magnetoelastic properties and the magnetization of the CoFe alloy. Due to the nanocrystalline structure of our electrodeposited CoFe alloy films, the choice of nonlinear isotropic for the magnetostriction model is the more appropriate one. In this model, the magnetomechanical strain and stress are as follows:

$$\varepsilon_{me} = \frac{3}{2}\frac{\lambda_S}{M_S^2} dev(\boldsymbol{M} \otimes \boldsymbol{M}) \quad (10)$$

where ε_{me} is the magnetostrictive strain tensor, λ_S is the saturation magnetostriction, M_S is the saturation magnetization, and dev($\boldsymbol{M} \otimes \boldsymbol{M}$) is the deviatoric second order magnetization tensor. Similarly, the stress in the magnetostrictive material is modeled as

$$S = c_H[\varepsilon - \varepsilon_{me}(M)] \quad (11)$$

where $c_H = c_H(E, \nu)$ is the stiffness matrix using Young's modulus and Poisson's ratio for isotropic materials.

Nonlinear magnetization is expressed by a nonlinear implicit relation:

$$\boldsymbol{M} = M_S L(|\boldsymbol{H}_{eff}|) \frac{\boldsymbol{H}_{eff}}{|\boldsymbol{H}_{eff}|} \quad (12)$$

where L is the Langevin functon:

$$L = \coth\left(\frac{3\chi_m|\boldsymbol{H}_{eff}|}{M_S}\right) - \frac{M_S}{3\chi_m|\boldsymbol{H}_{eff}|} \quad (13)$$

and the effective magnetic field, $\boldsymbol{H}_{eff}$, is a combination of both magnetic and magnetostrictive components.

$$\boldsymbol{H}_{eff} = \boldsymbol{H} + \frac{3\lambda_S}{\mu_0 M_S^2} S_{ed} \boldsymbol{M} \quad (14)$$

S_{ed} = dev($c_H\varepsilon$) is the deviatoric stress tensor, χ_m is the magnetic susceptibility in the initial linear region of the B-H curve and μ_0 is the vacuum permeability.

A second Ampère's law node, Ampère's Law, Magnetostrictive 1, is added under the Magnetic Fields (*mf*) interface. In this node, the magnetization and the magnetic field add to give the magnetic flux density:

$$\boldsymbol{B} = \mu_0(\boldsymbol{H} + \boldsymbol{M}) \quad (15)$$

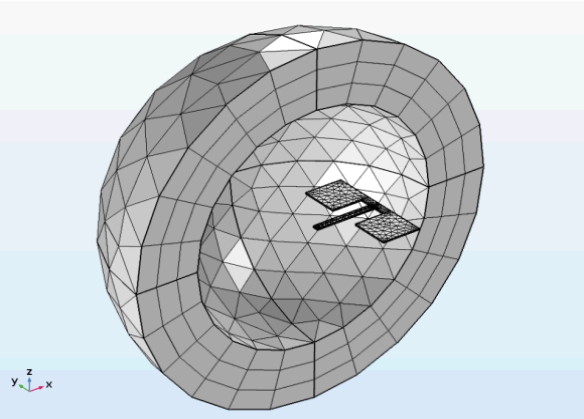

Figure 2. Mesh used for magnetoelastic actuation model.

3.3. Meshing

Bilateral symmetry was exploited in this model to reduce the number of nodes. Only half of each capacitor was modeled with the axis of symmetry running down the center of the cantilever. Similarly, a hemispherical air volume with Infinite Element domains was used to approximate a very large distance from the region of interest. The generated

mesh is shown in Figure 2. For the purposes of visual clarity, a full cantilever plus hemispherical air volume with all the air domains hidden is used in the figure. A user controlled mesh was applied to the model. Free tetrahedrals with a size set to "Normal" were applied to the CoFe film, the copper, and the air volume. A swept mesh was applied to the Infinite Element domains with a fixed number of elements set to three. This configuration gives a mesh quality of approximately 0.6.

3.4. Study

A stationary study was used to model the capacitor with the MUMPS solver. Parametric sweeps were first used to determine an optimal thickness for both copper and CoFe materials for a λ_S range between 50 and 100 ppm at $B = 1$ T for MEMS Cap 1. The intent was to magnetically saturate the film without the capacitor top plate touching the bottom plate resulting in a short before reaching a value of $\lambda_S = 100$ ppm. This resulted in a thickness of 2 μm for CoFe and 9 μm for copper that are both compatible with achievable photoresist molds for electroplated films. Finally, setting λ_S to 100 ppm, a magnetic flux sweep was performed to determine the displacement of the cantilever tip and the resulting capacitance change between 0 and 1 T.

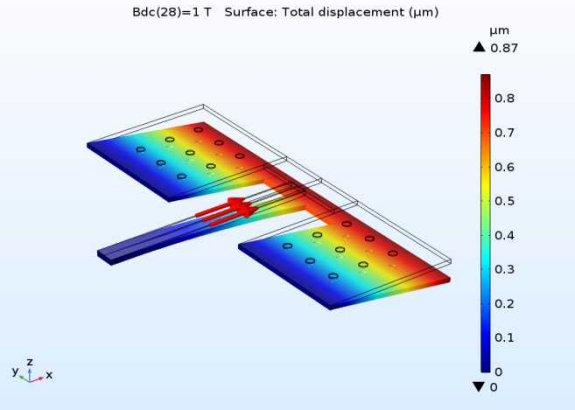

Figure 3. Total displacement of MEMS Cap 1.

4. Simulation Results

Figure 3 shows a surface displacement plot for MEMS Cap 1. The displacement is given at $B = 1$ T with λ_S set to 100 ppm. Red arrows show the direction of applied flux parallel to the easy axis of the CoFe alloy film in the undeflected capacitor structure represented by a transparent wire frame. This results in a downward displacement of the free end of the capacitor towards the bottom capacitor plate not shown in the figure. This is expected for a positive magnetostrictive material which tries to expand while the copper remains unaffected by the applied magnetic flux.

Figure 4 plots the results of capacitance and capacitor gap with respect to the cantilever tip as a function of applied magnetic flux density. Capacitance in this model is determined by performing a line integral along the width (x-direction) of the top capacitor plate of a particular design.

$$C = \sum_{i=0}^{n} \alpha \varepsilon_0 depth \int_0^{width} \frac{dx}{1+w} \qquad (16)$$

where the capacitance, C, is the sum of blocks used to comprise the capacitor top plate, n is the number of different type of blocks used, α is a number that reflects if symmetry is used and can be 1 or more depending on how the geometry is set up, ε_0 is the vacuum permittivity, *depth* is the block dimension along the y-direction, *width* is the block dimension along the x-direction, and w is the z-displacement along the x-direction and is a negative value in this case.

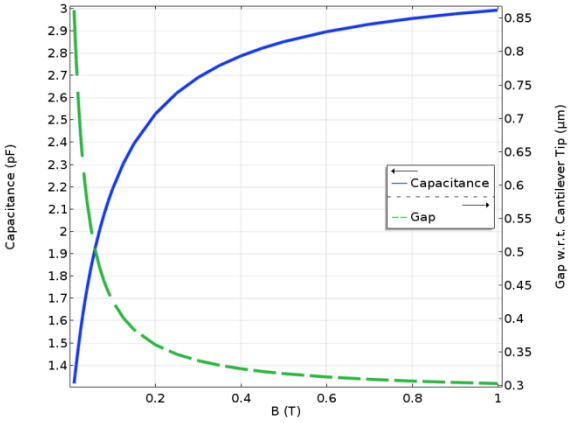

Figure 4. Capacitance and gap spacing as a function of applied magnetic flux density

The angle formed by the top and bottom plates during displacement is ignored in this calculation as it constitutes less than 1% error to the total value.
The best metric for evaluating device performance is by it's sensitivity. If you look at the quasilinear portion of the curve between B = 0.01 to 0.1 T in Figure 4, you get a cantilever tip displacement range from 0.14 to 0.57 μm over a capacitance range of 1.3 to 2.2 pF. This gives a sensitivity of 0.48 μm/pF. This allows it to span the range of λ_S between 1 ppm and 100 ppm. Given the sub-pF resolution of our LCR meter, this should allow us better than 1 microstrain sensitivity. While not as good as nanostrain sensivities of typical laser systems, it is still better than most resistive strain gauges that have a strain resolution of ± 5 microstrain.

Since cantilever tip displacement is what we ultimately need to make use of Equation 1 and

capacitance is what we'll actually be measuring, a more useful way to plot the data in Figure 4 is cantilever tip displacement vs capacitance as shown in Figure 5.

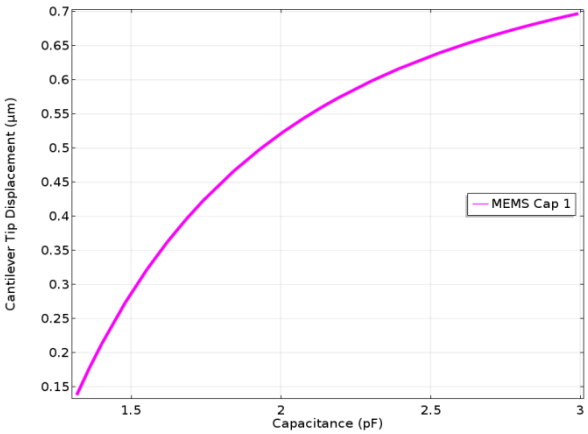

Figure 5. Cantilever tip displacement vs capacitance.

This plot also provides a means of measuring cantilever tip displacement regardless of what thickness combination of CoFe alloy to copper is used as long as the other design dimensions remain the same.

5. Conclusion

This paper presents a COMSOL model of a novel MEMS variable capacitor for measuring magnetostriction in electroplated films as a function of applied magnetic field. This model will be used to generate design criteria for real capacitors created through microfabrication. MEMS Cap 1 has a sensitivity of 0.48 µm/pF that can cover a range of 1 to 100 ppm of magnetostriction for a given geometry and material thickness. Sensitivities and magnetostriction ranges are subject to change with different geometries and thicknesses for films possessing higher degrees of magnetostriction. Finally, a plot of cantilever tip displacement vs. capacitance was generated from which future measurements of different magnetostrictive alloy films can be measured.

References

1. R. Osiander, S. A. Ecelberger, R. B. Givens, D. K. Wickenden, J. C. Murphy, and T. J. Kistenmacher, "A microelectromechanical-based magnetostrictive magnetometer," Applied Physics Letters, vol. 69, pp. 2930-2931, 1996.
2. C. Body, G. Reyne, G. Meunier, E. Quandt, and K. Seemann, "Application of magnetostrictive thin films for microdevices," Magnetics, IEEE Transactions on, vol. 33, pp. 2163-2166, 1997.
3. D. Hunter, W. Osborn, K. Wang, N. Kazantseva, J. Hattrick-Simpers, R. Suchoski, R. Takahashi, M. L. Young, A. Mehta, L. A. Bendersky, 4. S. E. Lofland, M. Wuttig, and I. Takeuchi, "Giant magnetostriction in annealed Co1−xFex thin-films," Nat Commun, vol. 2, p. 518, 2011.
4. R. R. Basantkumar, B. J. Stadler, W. P. Robbins, and E. Summers, "Integration of Thin-Film Galfenol with MEMS Cantilevers for Magnetic Actuation," in Magnetics Conference, 2006. INTERMAG 2006. IEEE International, 2006, pp. 459-459.
5. Y. Hui, T. Nan, N. X. Sun, and M. Rinaldi, "High Resolution Magnetometer Based on a High Frequency Magnetoelectric MEMS-CMOS Oscillator," Microelectromechanical Systems, Journal of, vol. PP, pp. 1-1, 2014.
6. G. Scheerschmidt, K. J. Kirk, and G. McRobbie, "Investigation of Magnetostrictive Microdevices," Ieee Transactions on Magnetics, vol. 43, pp. 2722-2724, 2007.
7. T. Jun, S. R. Green, and Y. B. Gianchandani, "Miniaturized magnetoelastic tags using frame-suspended hexagonal resonators," in Micro Electro Mechanical Systems (MEMS), 2014 IEEE 27th International Conference on, 2014, pp. 76-79.
8. E. du Trémolet de Lacheisserie and J. C. Peuzin, "Magnetostriction and internal stresses in thin films: the cantilever method revisited," Journal of Magnetism and Magnetic Materials, vol. 136, pp. 189-196, 1994.

Acknowledgements

This project was supported by Laboratory Directed Research and Development (LDRD) Project numbers 150356 and 200169. Sandia National Laboratories is a multimission laboratory managed and operated by National Technology and Engineering Solutions of Sandia, LLC, a wholly owned subsidiary of Honeywell International, Inc., for the U.S. Department of Energy's National Nuclear Security Administration under contract DE-NA0003525.

Appendix

Appendix 1. Material properties used in COMSOL model.

Properties/Material	Copper	$Co_{70}Fe_{30}$	Air
Electrical Conductivity (S/m)	5.998e7	4.81e6	0
Relative Permittivity	1	1	1
Saturation Magnetization (A/m)	0	1.58e6	-
Saturation Magnetostriction	0	78e-6	-
Magnetic Susceptibility	0	165.6	0
Density (kg/m^3)	8700	8551	-
Young's Modulus (Pa)	110e9	139e9	-
Poisson's Ratio	0.35	0.3	-